



Original Article

Asian Pacific Journal of Tropical Biomedicine



apjtb.org

doi: 10.4103/apjtb.apjtb_83_25

Auranofin amplifies schisandrin A-induced apoptosis through ROS generation and inhibiting the PI3K/Akt pathway in hepatocellular carcinoma

Hyun Hwangbo^{1,2✉}, Seon Yeong Ji^{1,2}, Min Yeong Kim^{1,2}, Su Hyun Hong^{1,2}, Sung Ok Kim³, Gi-Young Kim⁴, Yung Hyun Choi^{1,2✉}¹Department of Biochemistry, Dong-eui University College of Korean Medicine, Busan 47227, Korea²Basic Research Laboratory for the Regulation of Microplastic-Mediated Diseases and Anti-Aging Research Center, Dong-eui University, Busan 47227, Korea³Department of Food and Nutrition, College of Life and Health, Kyungsung University, Busan 48434, Korea⁴Department of Marine Life Science, Jeju National University, Jeju 63243, Korea

ABSTRACT

Objective: To investigate the synergistic effects of auranofin and schisandrin A (SA) on cell proliferation inhibition and apoptosis induction in human hepatocellular carcinoma Hep3B cells.

Methods: Cell viability was assessed using MTT to determine the synergistic effects of auranofin and SA. Three-dimensional (3D) culture models were used to evaluate the effects on spheroid structure and size. Apoptosis was analyzed by flow cytometry for sub-G₁ populations, annexin V staining, and Western blotting for apoptotic markers. Reactive oxygen species (ROS) production was measured using DCF-DA staining.

Results: Our results showed that combined treatment with auranofin and SA led to a significant reduction in cell viability compared with either compound alone, with isobologram analysis confirming their synergistic interactions. Under 3D culture conditions, auranofin and SA disrupted the compact structure of spheroids, leading to a loosened and disorganized morphology at the periphery, which appeared as an increase in spheroid size. Moreover, the induction of apoptosis by auranofin and SA was evidenced by elevated sub-G₁ phase populations, increased annexin V-positive cells, and upregulation of apoptotic markers such as cleaved poly (ADP-ribose) polymerase 1 and cleaved caspase-3. Notably, auranofin combined with SA markedly enhanced ROS production, which was mitigated by the ROS scavenger *N*-acetylcysteine. Additionally, the phosphoinositide 3-kinase (PI3K)/Akt signaling pathway was downregulated in response to auranofin and SA treatment, and further apoptotic effects were observed following PI3K inhibition with LY294002.

Conclusions: Auranofin combined with SA promotes apoptosis of

hepatocellular carcinoma *via* ROS generation and inhibition of the PI3K/Akt pathway.

KEYWORDS: Auranofin; Apoptosis; Hepatocellular carcinoma; Reactive oxygen species; Schisandrin A; PI3K/Akt

Summary

Question: Does the combination of auranofin and schisandrin A enhance apoptosis in hepatocellular carcinoma Hep3B cells by modulating ROS and PI3K/Akt signaling?

Findings: In this *in vitro* study using 2D and 3D spheroid models, the combination of auranofin and schisandrin A significantly increased ROS levels and apoptosis in Hep3B cells while downregulating PI3K/Akt signaling. ROS scavenger treatment reversed these effects, confirming ROS as a key mediator.

Meaning: These findings suggest that targeting ROS with auranofin and schisandrin A could be a promising therapeutic approach for hepatocellular carcinoma cells by inducing apoptosis through oxidative stress modulation.

✉To whom correspondence may be addressed. E-mail: hhyun@deu.ac.kr (H. Hwangbo); choiyh@deu.ac.kr (YH. Choi)

This is an open access journal, and articles are distributed under the terms of the Creative Commons Attribution-Non Commercial-ShareAlike 4.0 License, which allows others to remix, tweak, and build upon the work non-commercially, as long as appropriate credit is given and the new creations are licensed under the identical terms.

For reprints contact: reprints@medknow.com

©2025 Asian Pacific Journal of Tropical Biomedicine Produced by Wolters Kluwer-Medknow.

How to cite this article: Hwangbo H, Ji SY, Kim MY, Hong SH, Kim SO, Kim GY, et al. Auranofin amplifies schisandrin A-induced apoptosis through ROS generation and inhibiting the PI3K/Akt pathway in hepatocellular carcinoma. Asian Pac J Trop Biomed 2025; 15(6): 239-250.

Article history: Received 6 March 2025; Revision 5 April 2025; Accepted 27 April 2025; Available online 23 May 2025

1. Introduction

Hepatocellular carcinoma (HCC) is one of the most prevalent and fatal forms of liver cancer[1,2]. Despite advances in early detection and treatment, the prognosis for patients with advanced HCC remains poor. Current therapeutic options, such as surgical resection, liver transplantation, and systemic treatments such as sorafenib, offer limited efficacy and significant toxicity[3,4]. These limitations emphasize the urgent need for safer and more effective therapeutic strategies to enhance patient outcomes and quality of life.

Recent research has increasingly focused on combining natural compounds with established anticancer drugs as a promising approach to enhance therapeutic efficacy against HCC[5,6]. Natural compounds derived from plants, marine organisms, and other sources have been shown to possess diverse biological functions, including antioxidant, anti-inflammatory, and anticancer properties[7,8]. Compounds, such as curcumin, resveratrol, and epigallocatechin gallate, have been extensively studied for their ability to inhibit cancer cell proliferation, induce apoptosis, and sensitize cancer cells to established therapies[9–11]. Natural compounds can be combined with existing drugs to overcome drug resistance by targeting multiple signaling pathways and reducing the side effects associated with high concentrations of chemotherapy[12]. While HCC remains an unsolved problem in oncology, with the existing treatments offering only modest benefits and often causing substantial toxicity, combining natural compounds with established anticancer drugs represents a promising path for the development of more effective and less toxic therapies for HCC. Ongoing studies are essential for a comprehensive understanding of combination therapies and clinical practice. Auranofin, a gold-containing compound used to effectively treat rheumatoid arthritis, is gaining attention as a promising candidate for cancer treatment owing to its ability to induce cell death[13]. Auranofin exerts its anticancer effects primarily by inhibiting thioredoxin reductase, a key enzyme involved in maintaining the cellular redox balance; it is recognized as a candidate drug for anticancer treatment in malignant tumors because it induces oxidative stress and apoptosis by disrupting the cellular redox balance[13,14]. Despite these promising attributes, the potential of combination therapy with auranofin for HCC treatment has not been fully explored. One compound of interest is schisandrin A (SA), a lignan derived from the fruit of *Schisandra chinensis*, which is widely used in traditional Korean medicine[15]. SA is well-known for its potent antioxidant properties and ability to modulate various biological pathways involved in inflammation, oxidative stress, and apoptosis[16,17]. The mechanisms by which SA exerts these effects are thought to involve the modulation of multiple signaling pathways, including the mitogen-activated protein kinase and phosphoinositide 3-kinase (PI3K)/Akt pathways, which are critical for cell survival and proliferation[18,19].

Reactive oxygen species (ROS) comprise various molecules, including hydrogen peroxide (H_2O_2), superoxide anion (O_2^-), hydroxyl radical ($\bullet OH$), and singlet oxygen (1O_2)[20]. ROS plays important roles in cellular signaling and immune responses, influencing processes such as cell growth, differentiation, and apoptosis[21]. However, excessive ROS accumulation can lead to oxidative stress, which is linked to diseases such as inflammation, aging, and cancer[22,23]. Owing to their impact on cell survival and death, ROS are considered the key mechanisms of anticancer activity through the induction of apoptosis. Additionally, ROS regulation is crucial for overcoming multidrug resistance in cancer and managing inflammatory diseases[24]. In particular, basal ROS levels are higher in cancer cells than in normal cells because of an imbalance between oxidants and antioxidants and a high metabolic rate[25]. Previous studies have shown that auranofin exerts its anti-lymphoma effect through potent ROS generation mediated by thioredoxin reductase[26]. Conversely, SA protects normal cells from oxidative stress caused by ROS by modulating the Nrf2 signaling pathway[27]. We investigated the outcomes of utilizing these two types of compounds, which have distinct propensities for ROS generation, within the specific environment of cancer cells.

This study explored the use of auranofin and SA based on their potential for synergistic interactions, with the aim of enhancing efficacy while minimizing toxicity. In particular, the combined effects of auranofin and SA on Hep3B HCC cells were investigated to gain valuable insights into their potential as a treatment strategy for HCC.

2. Materials and methods

2.1. Cell culture and treatment

Hep3B cells were purchased from the American Type Culture Collection (ATCC, Manassas, VA, USA) and cultured in Dulbecco's Modified Eagle's Medium (Welgene Inc., Gyeongsan, South Korea) supplemented with 10% fetal bovine serum and 1% penicillin-streptomycin. The cells were maintained in a 37 °C humidified 5% CO₂ environment. Auranofin and SA were obtained from Sigma-Aldrich (St. Louis, MO, USA), dissolved in dimethyl sulfoxide (Generay, Shanghai, China) at concentrations of 1 and 100 mM, respectively, and stored at –80 °C until use.

2.2. Cell viability assay

Hep3B cells were seeded at 1.5×10^5 cells/well in six-well plates and incubated for 24 h. After stabilizing, the cells were exposed to 1 μM auranofin and various concentrations (50, 100, and 200 μM) of SA in a fresh medium for 24 h. In addition, LY294002 (5 μM), as an inhibitor of

PI3K/Akt signaling pathway, was pretreated for 1 h. Next, the cells were incubated with 3-(4,5-dimethylthiazol-2-yl)-2,5-diphenyltetrazolium bromide (MTT) solution (Thermo Fisher Scientific, Waltham, MA, USA) at a final concentration of 0.5 mg/mL[28]. To form formazan, the reaction was conducted at 37°C for 2 h, and absorbance was measured at 540 nm after dissolving formazan in dimethyl sulfoxide.

2.3. Colony formation assay

Cells exposed to auranofin (1 μ M) and SA (200 μ M) were seeded in six-well plates at a density of 2000 cells/well. The cells were incubated at 37°C for 12 d, and replaced with a fresh medium every 3 days. After colony proliferation, the colonies were washed with phosphate-buffered saline and fixed with 4% formaldehyde (Junsei Chemical Co., Tokyo, Japan) for 30 min at room temperature. The colonies were then stained with 0.05% crystal violet (Sigma-Aldrich), followed by washing with phosphate-buffered saline. The stained colonies were observed under a phase-contrast microscope (Carl Zeiss, Oberkochen, Germany), and the number of colonies was analyzed using Image J software (version 1.52a; National Institutes of Health, Bethesda, MD, USA).

2.4. Apoptosis analysis

Apoptosis was analyzed by measuring annexin V positivity and the population in the sub-G₁ phase for cells treated with the indicated concentrations of auranofin and SA. Briefly, the cells were harvested and stained with FITC annexin V/propidium iodide (PI) Apoptosis Detection Kit (BD Biosciences, Franklin Lakes, NJ, USA) and BD Cycletest™ Plus DNA Reagent Kit (BD Biosciences), respectively, and analyzed with an Accuri C6 Plus flow cytometer (BD Biosciences)[29].

2.5. Evaluation of mitochondrial membrane potential (MMP, $\psi\Delta m$)

To estimate loss of MMP ($\psi\Delta m$) by apoptosis, the cells treated with auranofin and SA were collected and incubated with JC-1 dye (10 μ M, Sigma-Aldrich) for 20 min. Following staining, green/red fluorescence ratio was analyzed using an Accuri C6 Plus flow cytometer[30].

2.6. ROS production

Intracellular ROS production following auranofin and SA treatment was detected using 2',7'-dichlorodihydrofluorescein diacetate (H₂DCFDA; Sigma-Aldrich), which emits green fluorescence depending on the redox state. *N*-Acetylcysteine (NAC) was used as a positive control for ROS scavenging. Cells were incubated with H₂DCF-DA for 20 min before harvesting. After incubation,

the stained cells were analyzed using an Accuri C6 Plus flow cytometer[31].

2.7. Western blot analysis

Briefly, total protein was extracted from Hep3B cells using a lysis buffer containing NaCl, Tris-Cl (pH 7.5), ethylene-diamine-tetraacetic acid, NP-40, 4-benzene sulfonyl fluoride hydrochloride, dithiothreitol, and a protease inhibitor cocktail (Sigma-Aldrich). Equal amounts of protein (30 μ g) were separated by sodium dodecyl sulfate-polyacrylamide gel electrophoresis and transferred onto nitrocellulose membranes (GE Healthcare, Chicago, IL, USA). The membranes were then incubated with the primary antibodies at 4°C overnight, followed by secondary antibodies at room temperature for 1 h[32]. Primary antibodies were purchased from Santa Cruz Biotechnology Inc. (Dallas, TX, USA) and Cell Signaling Technology (Danvers, MA, USA) (Supplementary Table). Secondary antibodies were purchased from Santa Cruz Biotechnology Inc. Finally, the proteins were visualized using enhanced chemiluminescence (ECL; Thermo Fisher Scientific) and detected using a Fusion Solo system (Vilber Lourmat, Collégien, France). Densitometric analysis of the Western blot bands was performed using ImageJ software. The intensity of the bands was quantified and normalized to the loading control for relative comparison.

2.8. Tumor spheroid formation assay

To generate HCC spheroids, 7×10^3 Hep3B cells were seeded onto a PrimeSurface three-dimensional (3D) culture plate (S-Bio, Siheung, South Korea) and stabilized for 3-5 d. The existing medium was carefully removed and replaced with a fresh medium containing auranofin (1 μ M) and SA (200 μ M). Tumor spheroid images were taken daily after auranofin and SA treatment, and their sizes were analyzed using ImageJ. H₂DCFDA staining was used to detect the ROS levels in Hep3B spheroids. Tumor spheroids were fixed with 4% formaldehyde, reacted with H₂DCFDA in an incubator for 20 min, stained with 4',6-diamidino-2-phenylindole (DAPI; Sigma-Aldrich), and observed under a fluorescence microscope (EVOS FL Auto 2; Thermo Fisher Scientific).

2.9. Statistical analysis

The data were presented as mean \pm standard deviation (SD) of at least three independent experiments. For multiple group comparisons, statistical significance was assessed using a one-way analysis of variance (ANOVA), followed by Tukey's *post hoc* test. The criterion for statistical significance was set at $P < 0.05$. All statistical analyses were performed using GraphPad Prism v8.4.2 (GraphPad Software., La Jolla, CA, USA).

3. Results

3.1. Auranofin and SA synergistically inhibit Hep3B cell proliferation

To evaluate the synergistic effect of auranofin and SA on the inhibition of Hep3B cell proliferation, the cells were treated with each chemical alone and cell viability was measured using the MTT assay (Figure 1A and B). Based on the results, the concentration that did not significantly reduce cell viability was selected for further experiments. To investigate the synergistic effects of auranofin and SA, cells were simultaneously treated with both chemicals and incubated for 24 h. The viability of Hep3B cells was significantly reduced by combined treatment with 1 μ M of auranofin and various concentrations (50, 100, and 200 μ M) of SA (Figure 1C). The isobologram confirmed that combined treatment with auranofin and SA had a synergistic effect (Figure 1D). Inhibition of colony

formation (Figure 1E) and reduced cell density (Figure 1F) were also observed. The inhibitory effects of auranofin and SA on cell proliferation were evaluated under 3D-culture conditions. As shown in Figure 1G, spheroids were firmly formed using Hep3B cells (Day 0). However, after 3 days of treatment with auranofin and SA, the outer surface of the spheroids was scattered compared to that of the control group, which remained firmly maintained. Accordingly, the area and size of the spheroids were also increased by auranofin and SA treatment (Figure 1H and I). Therefore, the combination treatment of auranofin and SA synergistically suppressed Hep3B cell growth and altered spheroid structure.

3.2. Auranofin combined with SA induces apoptosis in Hep3B cells

As shown in Figure 2A and C, auranofin and SA treatment significantly increased the population of cells in the sub-G₁ phase.

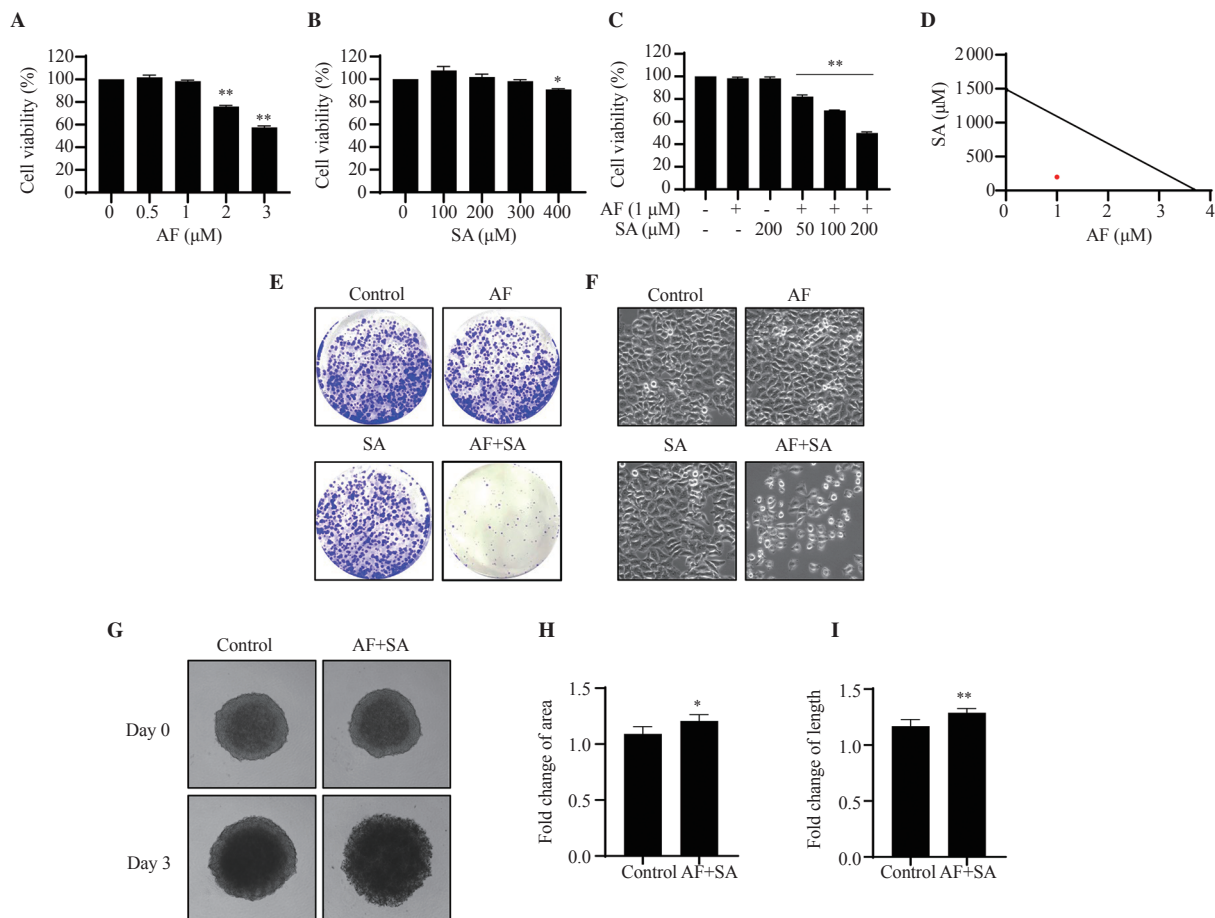


Figure 1. Effects of auranofin and schisandrin A (SA) on the proliferation and growth of Hep3B cells and spheroids. Cells were treated with auranofin and SA alone or together at the indicated concentrations for 24 h. (A–C) Cell viability was determined by MTT assay. Data are expressed as mean \pm SD of three independent experiments. * P <0.05 and ** P <0.001 compared with the control group. (D) Isobologram was calculated based on the cell viability. (E) Colonies formed after incubation with auranofin and SA were stained with 0.05% crystal violet. (F) Representative phase-contrast images of morphology. (G) Representative phase-contrast images of 3D spheroids treated with auranofin and SA for 3 days. The (H) area and (I) length of spheroids were quantified using ImageJ. * P <0.05 and ** P <0.001 compared with the control group on Day 3. AF: auranofin.

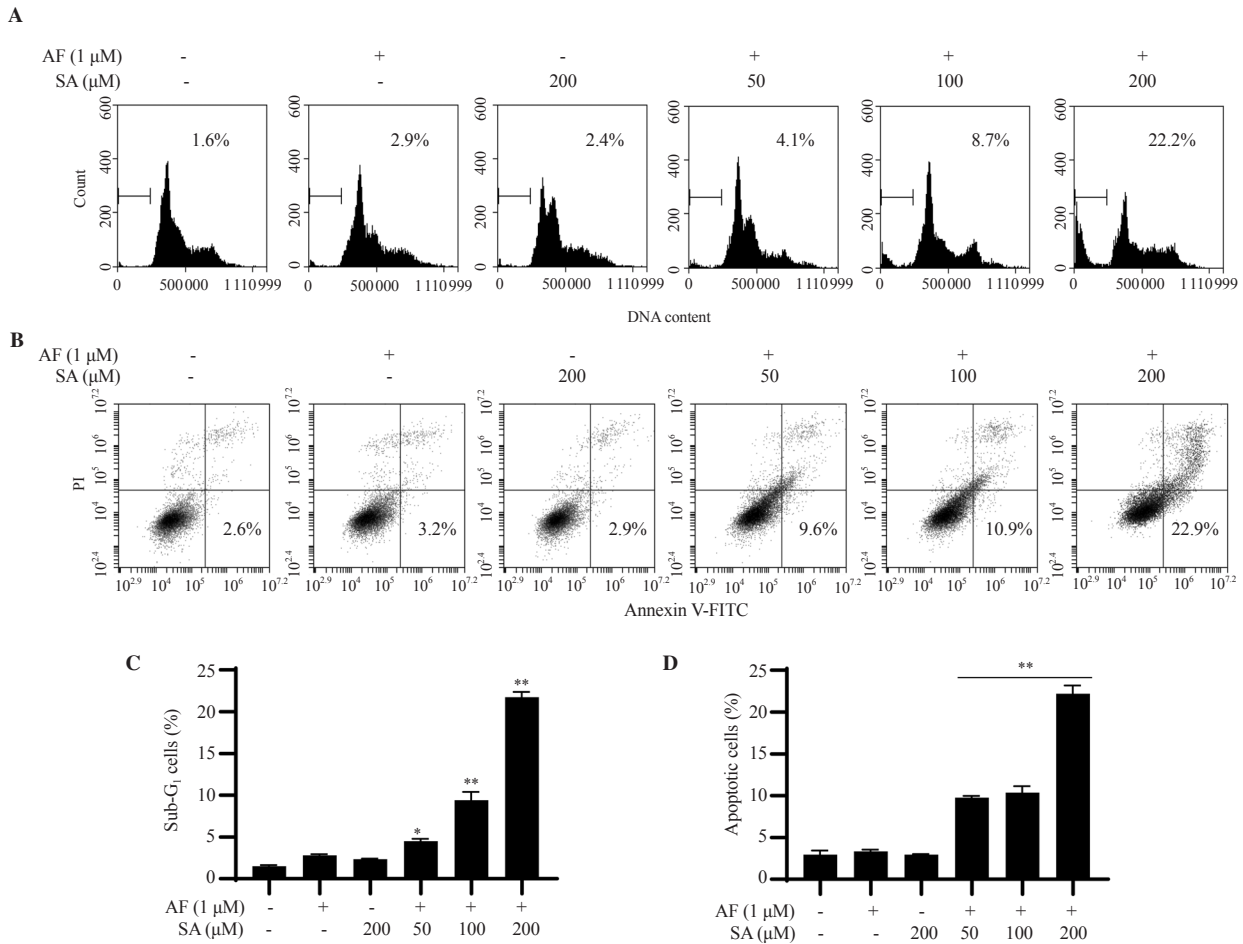


Figure 2. Auranofin and SA induce apoptosis in Hep3B cells. Cells were treated with indicated concentration of auranofin and SA for 24 h. Apoptosis induced by auranofin and SA was detected by (A and C) cell cycle and (B and D) annexin V-FITC/propidium iodide (PI) analysis using flow cytometry. Data are expressed as mean \pm SD of three independent experiments. * P <0.05 and ** P <0.001 compared with the control group.

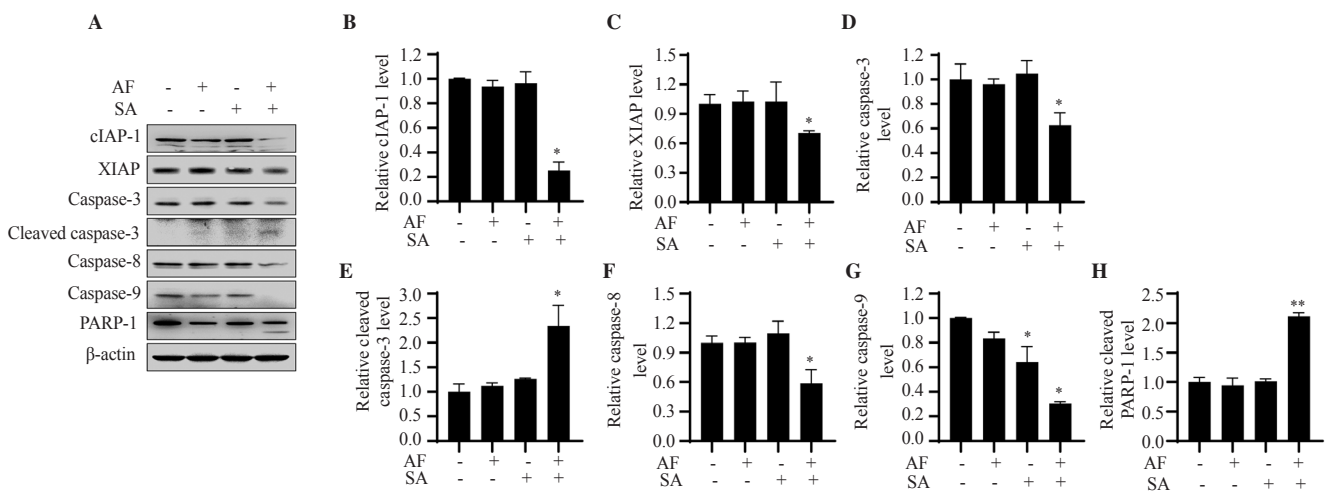


Figure 3. Expression levels of apoptosis-related factors after auranofin and SA treatment in Hep3B cells. Cells were exposed to auranofin (1 μ M) and SA (200 μ M) alone or in combination for 24 h. (A) Total protein was isolated from the cells and Western blot analysis was performed on the same amount of protein. β -actin was used as the loading control. Quantitative analysis of the expression of (B) cIAP-1, (C) XIAP, (D) caspase-3, (E) cleaved caspase-3, (F) caspase-8, (G) caspase-9, and (H) cleaved PARP-1. Data are expressed as mean \pm SD of three independent experiments. * P <0.05 and ** P <0.001 compared with the control group.

It was attributed to an increase in DNA fragmentation, a hallmark of apoptosis. Annexin V/PI double staining was used to detect apoptosis in Hep3B cells. The percentages of early and late apoptotic cells were markedly elevated after auranofin and SA treatment (Figure 2B and D). As shown in Figure 3, Western blot analysis indicated that the levels of caspase-3, -8, and -9, which play a major role in the initiation and execution of apoptosis, were decreased by auranofin and SA treatment. Additionally, the active forms of caspase-3 and cleaved poly(ADP-ribose) polymerase 1 (PARP-1), a known substrate of caspase-3, were significantly increased by auranofin and SA treatment. Treatment with auranofin and SA also decreased the expression of cIAP-1 and XIAP. Thus, auranofin and SA promoted apoptosis in Hep3B cells by elevating apoptotic markers and decreasing anti-apoptotic proteins.

3.3. Combined treatment with auranofin and SA triggers ROS production in Hep3B cells

The explosive accumulation of ROS presents a potential environment for the induction of apoptosis in cancer cells. Therefore, we assessed the intracellular ROS levels in 2D and 3D culture systems using H₂DCFDA staining. As shown in Figure 4A and B, the

level of ROS remarkably increased 1 h after treatment with auranofin and SA, which was reduced to the control level by NAC, a ROS scavenger. For Hep3B spheroids, H₂DCFDA fluorescence intensity was significantly increased by combined treatment of auranofin and SA, which was decreased by NAC treatment, consistent with the results in the 2D culture system (Figure 4C and D). The increased ROS levels induced by auranofin and SA in both 2D and 3D cultures were reversed by NAC, highlighting the role of ROS in the apoptotic effects of the treatment.

3.4. ROS is a key regulator of auranofin and SA-induced apoptosis in Hep3B cells

To determine whether ROS generation modulates auranofin- and SA-induced apoptosis, the cells were treated with NAC. As shown in Figure 5A, the auranofin and SA-induced reduction in cell viability was significantly restored by pretreatment with NAC in the 2D culture system. In 3D spheroids, NAC treatment partially firm the scattered outer surface, and the area and size were significantly reduced compared with auranofin and SA treatment without NAC (Figure 5B-D). In addition, NAC blocked auranofin and SA-induced apoptosis (Figure 5E and F). To quantify the damage to

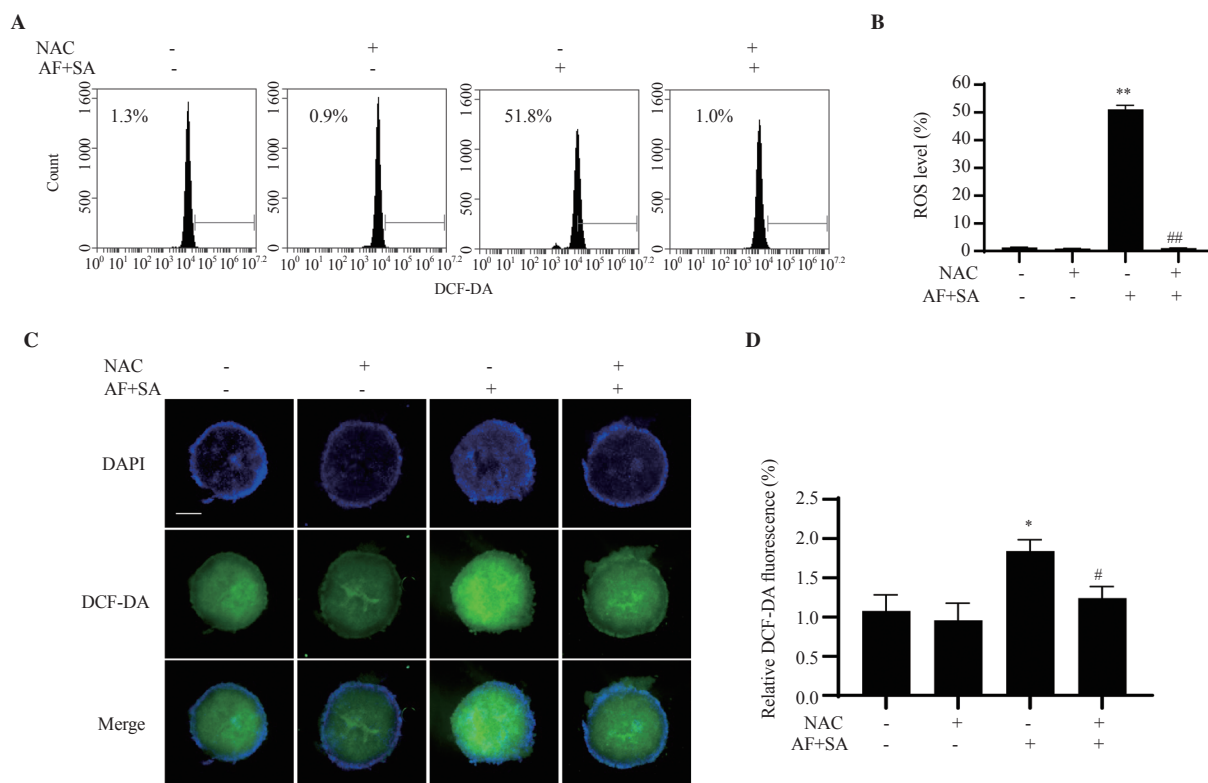


Figure 4. Effects of auranofin and SA treatment on ROS accumulation. (A and B) Cells were treated with auranofin (1 μ M) and SA (200 μ M) for 1 h. *N*-Acetylcysteine (NAC) (10 mM) was administered 1 h before auranofin and SA treatment. Intracellular ROS was detected using H₂DCFDA staining and flow cytometry. (C and D) Representative image of H₂DCFDA-stained spheroids on Day 3 after auranofin and SA treatment (scale bar = 500 μ m). Data are expressed as mean \pm SD of three independent experiments. * P <0.05 and ** P <0.001 compared with the control group; # P <0.05 and ### P <0.001 compared with the auranofin + SA group.

mitochondria during apoptosis, MMP ($\psi\Delta m$) was measured using JC-1 dye. Auranofin and SA-induced MMP loss was recovered by NAC treatment (Figure 5G and H). Overall, the effects of auranofin and SA on cell apoptosis and proliferation were abrogated by NAC, confirming the role of ROS in the apoptotic process.

3.5. The PI3K/Akt signaling pathway is downregulated in auranofin and SA-induced apoptosis

We evaluated protein expression using Western blot analysis and changes in apoptosis using the PI3K inhibitor. Expression levels of the total and phosphorylated forms of PI3K and Akt are shown in Figure 6A. Treatment with auranofin and SA led to a significant reduction in the expression of phosphorylated PI3K and Akt as well as cell viability, whereas LY294002 further amplified the effects of auranofin and SA. We then investigated the changes in auranofin- and SA-induced apoptosis after treatment with LY294002. As shown in Figure 6C-D, apoptotic cell death and MMP loss induced by

auranofin and SA were further aggravated by LY294002 treatment. Therefore, auranofin and SA reduced the levels of phosphorylated PI3K and Akt, and further inhibition of PI3K by LY294002 exacerbated apoptosis and mitochondrial damage, indicating the involvement of the PI3K/Akt pathway in their apoptotic effects.

3.6. ROS contributes to auranofin and SA-induced apoptosis by inhibiting the PI3K/Akt signaling pathway

To examine which factors are the main or preferential mechanisms of auranofin and SA-induced apoptosis, changes in apoptosis were measured following treatment with NAC and LY294002. Cell viability decreased by auranofin and SA treatment was restored by NAC and LY294002 co-treatment (Figure 7A). Additionally, apoptosis and MMP loss induced by auranofin and SA were reduced by both inhibitors (Figure 7B-E). These results demonstrate that ROS blockade, rather than the PI3K/Akt signaling pathway, was a critical factor in auranofin and SA-induced apoptosis. Consequently,

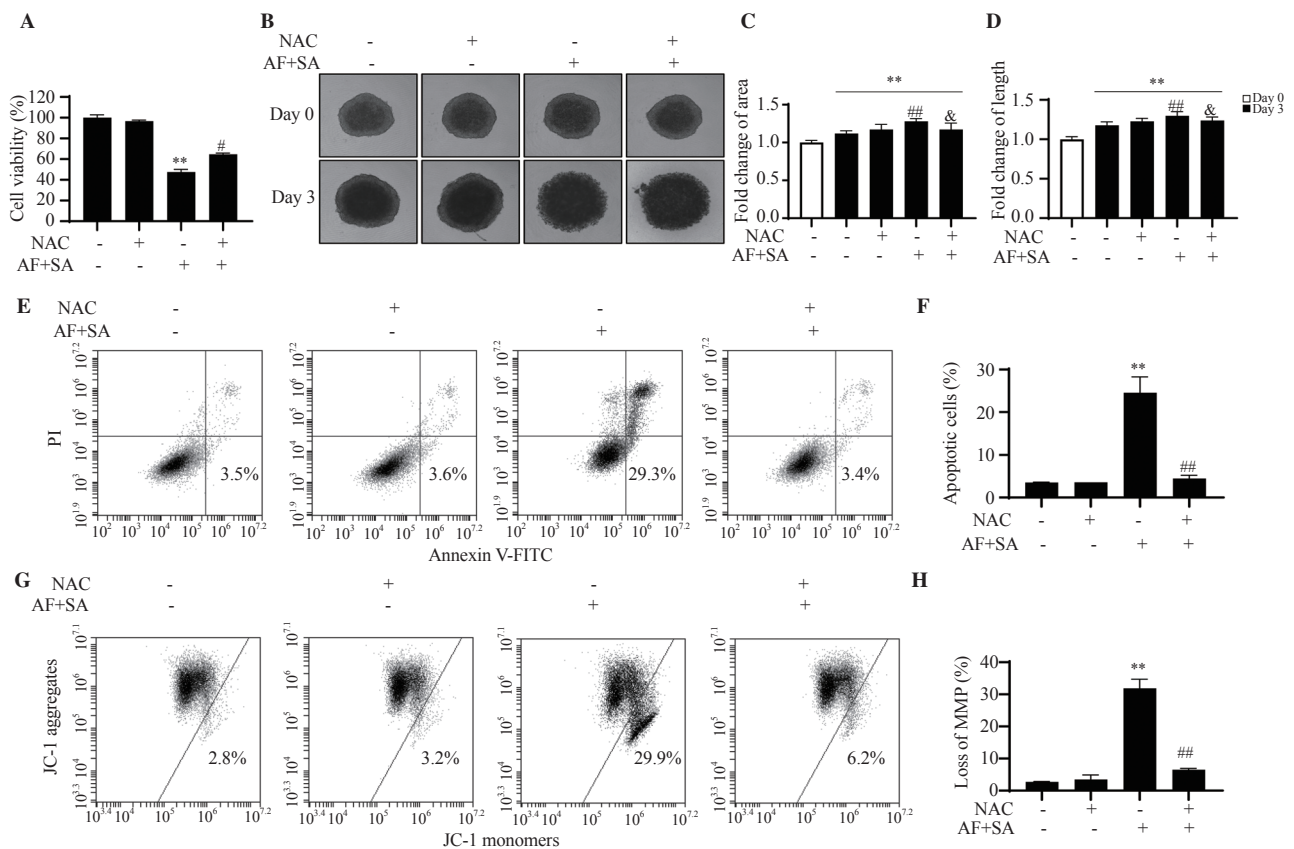


Figure 5. Changes in auranofin and SA-induced apoptosis by ROS regulation. Cells exposed to NAC (10 mM) for 1 h were treated with auranofin (1 μ M) and SA (200 μ M) for 24 h. (A) MTT assay was performed to investigate cell viability. ** P <0.001 compared with the control group; # P <0.05 compared with the auranofin + SA group. (B) Representative phase-contrast images of 3D spheroids. In the Hep3B-derived 3D spheroid, NAC treatment was applied for 3 days in the same manner as auranofin and SA. The (C) area and (D) length of spheroids were quantified using ImageJ. Data are expressed as mean \pm SD of three independent experiments. ** P <0.001 compared with the control group on Day 0; # P <0.05 and ## P <0.001 compared with the control group on Day 3; & P <0.05 compared with the auranofin + SA group. (E and F) Apoptotic cell death and (G and H) loss of MMP were analyzed using flow cytometry. Data are expressed as mean \pm SD of three independent experiments. ** P <0.001 compared with the control group; ## P <0.001 compared with the auranofin + SA group.

the restoration of cell viability and the reduction in apoptosis by NAC and LY294002 showed that ROS inhibition, rather than PI3K/Akt pathway modulation, was the primary mechanism of auranofin and SA-induced apoptosis.

4. Discussion

Synergistic inhibition of cancer cell proliferation is crucial because it enhances the effectiveness of treatment by simultaneously targeting multiple pathways. This combined treatment approach may enhance cancer cell growth inhibition and potentially reduce resistance, thereby improving therapeutic efficacy[33,34]. In this study, we explored the potential treatment of two or more compounds at low concentrations to induce cancer cell death and achieve an effective anticancer treatment for HCC.

Auranofin, a thioredoxin reductase inhibitor, exhibits anticancer activity by modulating the redox balance, inducing apoptosis, regulating cellular signaling, and activating the immune system[35,36].

Moreover, auranofin has been investigated in combination therapies for its potential to enhance synergistic effects, overcome drug resistance, offer a broad spectrum of action, and reduce toxicity[37,38]. SA has been reported to exhibit anticancer activity against breast, non-small cell lung, and colorectal cancers[17,39,40]. In liver cancer, the anticancer activity of SA is enhanced by destroying microbubbles using ultrasound, which increases cancer cell death and reduces tumor size[41]. Our results demonstrated a potent combinatorial effect of auranofin and SA for synergistic inhibition of Hep3B cell proliferation. The MTT assay and subsequent isobologram analysis showed that the combination treatment significantly reduced cell viability more effectively than either compound alone. These findings suggest that auranofin and SA act synergistically to impair cell growth *via* complementary mechanisms. To mimic the tumor microenvironment more accurately than 2D models, we used 3D spheroid models for a more precise evaluation of the combined effects of auranofin and SA in preclinical studies and to yield more realistic data. Our results demonstrated that the morphology of the 3D spheroids was altered, and their size increased, likely due to

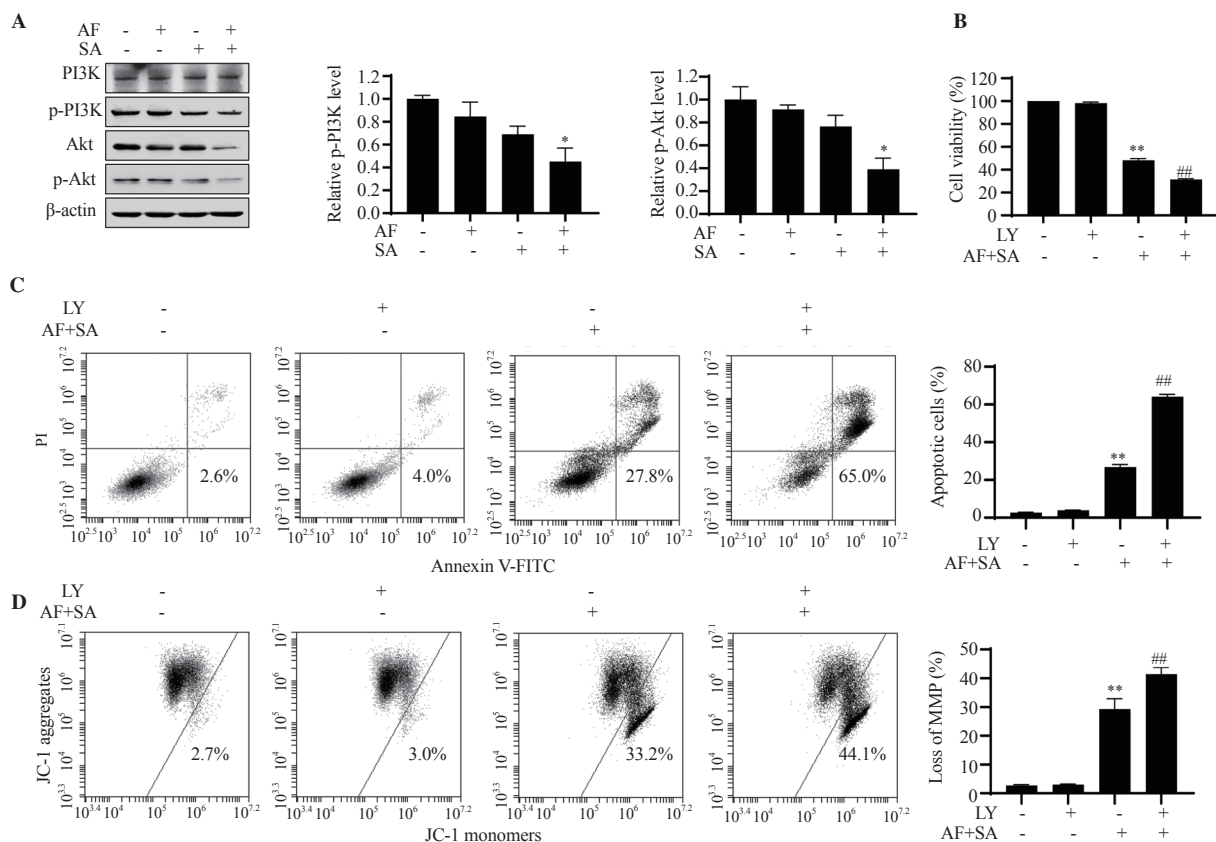


Figure 6. Suppression of the PI3K/Akt signaling pathway in auranofin and SA-induced apoptosis. (A) Cells were treated with auranofin (1 μ M) and SA (200 μ M) for 24 h. Expression levels of phosphorylated PI3K and Akt were determined using Western blot analysis. (B) Cell viability after incubation with PI3K inhibitor (LY294002; 5 μ M) was examined using MTT assay. (C) Annexin V-positive cells and (D) cells with MMP loss were quantified using flow cytometry. Data are expressed as mean \pm SD of three independent experiments. * P <0.05, ** P <0.001 compared with the control group; ## P <0.001 compared with the auranofin + SA group.

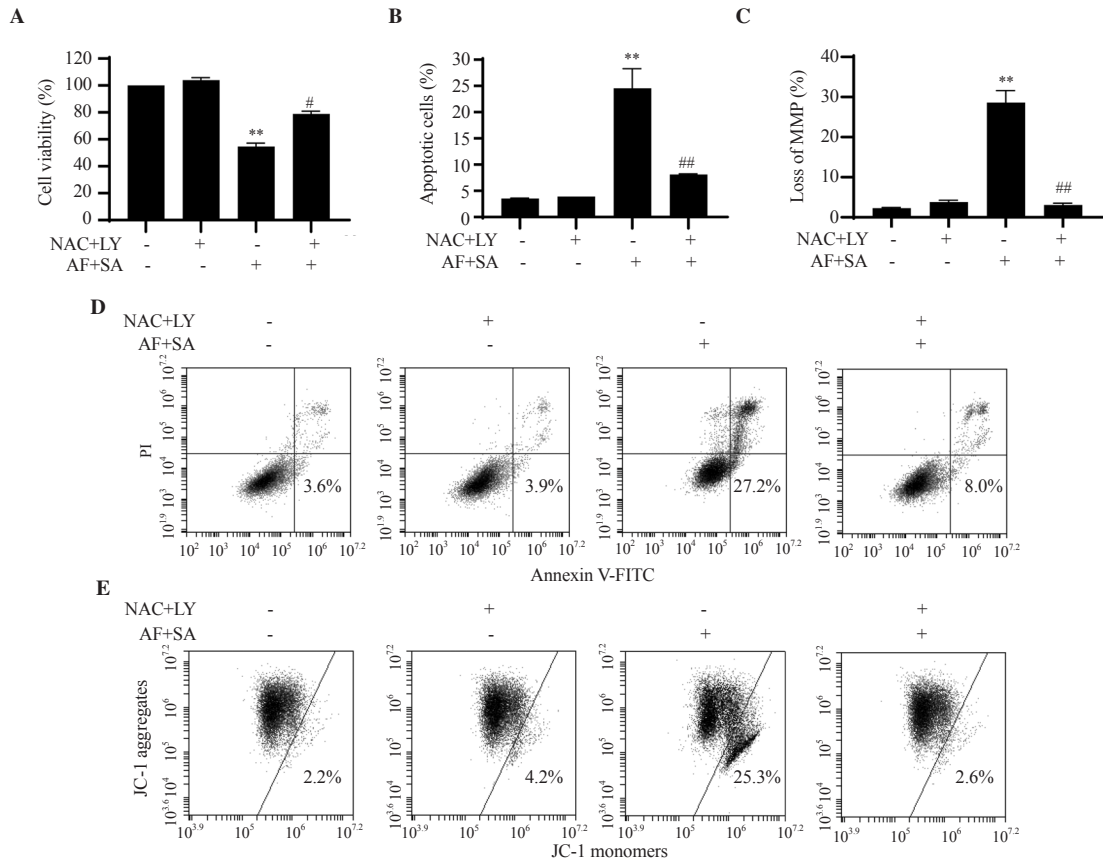


Figure 7. Role of ROS regulation in auranofin and SA-induced apoptosis *via* PI3K inhibition. Cells were treated with auranofin (1 μ M) and SA (200 μ M) for 24 h. NAC (10 mM) and PI3K inhibitor (5 μ M) were used for 1 h before auranofin and SA treatment. (A) Cell viability, (B and D) apoptotic cell death, and (C and E) loss of MMP were determined. Data are expressed as mean \pm SD of three independent experiments. ** P <0.001 compared with the control group; # P <0.05 and ## P <0.001 compared with the auranofin + SA group.

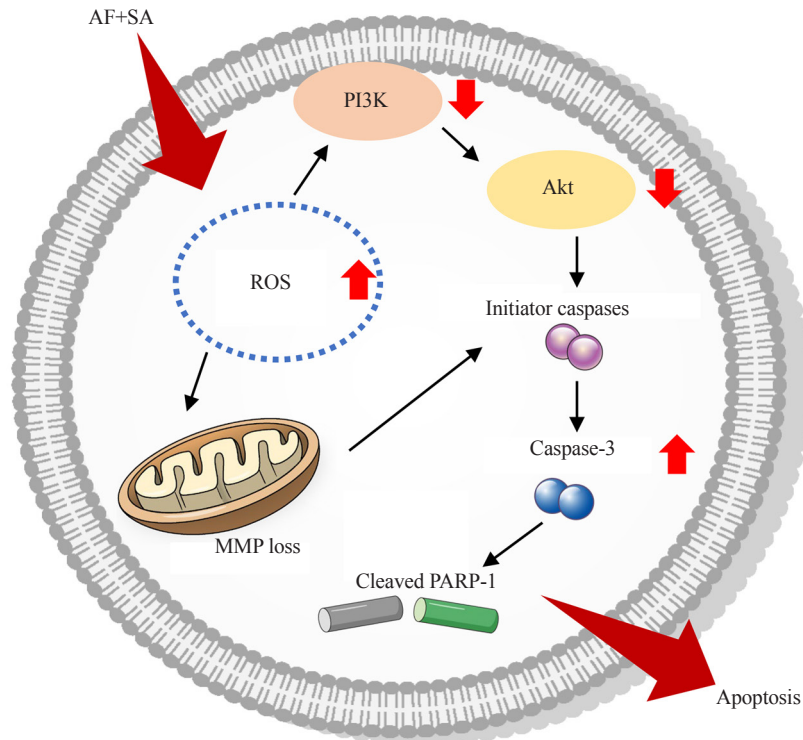


Figure 8. A schematic diagram showing that auranofin amplifies SA-induced apoptosis through ROS generation and inhibits the PI3K/Akt pathway in Hep3B cells.

structural disruptions and reduced intercellular adhesion, rather than enhanced cell proliferation. These changes suggest a destabilization of the spheroid structure, rather than an increase in cell growth. The induction of apoptosis by the combination of auranofin and SA was evidenced by increased sub-G₁ cell populations, enhanced annexin V/PI staining, and upregulated apoptotic markers such as cleaved PARP-1 and active caspase-3. These results indicated that the synergistic effect of auranofin and SA triggered cell death pathways. The downregulation of pro-caspases and reduced expression of IAP family proteins further supported that auranofin and SA enhanced apoptosis by modulating key apoptotic regulators. Given that the auranofin concentration used in this study was lower than that reported in previous studies, this approach may be more efficient, highlighting its potential therapeutic relevance[42,43].

Intracellular ROS induces apoptosis by generating oxidative stress that damages cellular components, including lipids, proteins, and DNA. Oxidative damage activates proapoptotic signaling pathways, disrupts mitochondrial function, and promotes the release of cytochrome c, leading to the activation of apoptosome and subsequent programmed cell death. Thus, ROS serves as both signals and mediators of the apoptotic process, connecting oxidative stress to cell death. Therefore, we investigated the ROS levels generated in response to auranofin and SA. Our findings showed that in 2D and 3D culture systems, the combined treatment significantly increased ROS production in Hep3B cells, and NAC treatment effectively restored cell viability and reduced cell death. These results indicated that ROS generation may play a key role in auranofin and SA-induced apoptosis. Enhanced ROS levels contribute to a proapoptotic environment that enables cell death, emphasizing the importance of oxidative stress in the mechanisms of action of auranofin and SA. These results are similar to those of previous studies, suggesting the role of ROS in apoptosis by blocking ROS in various cancer cells[44].

In cancer, the PI3K/Akt signaling pathway plays a key role in promoting cell survival, growth, and proliferation by inhibiting apoptosis, enhancing cellular metabolism, and contributing to resistance to various therapies. Several studies have suggested that the PI3K/Akt signaling pathway plays an important role in HCC metabolism and is a potential target for HCC treatment. Therefore, our study investigated the involvement of the PI3K/Akt signaling pathway in apoptosis induced by auranofin and SA. After treatment with the PI3K inhibitor LY294002, the downregulation of phosphorylated PI3K and Akt, along with the aggravation of cell death and loss of MMP, indicated that the PI3K/Akt pathway was involved in the response to auranofin and SA. The interplay between ROS generation and PI3K/Akt signaling was a key aspect of this study. Co-treatment with NAC (ROS inhibitor) and LY294002 (PI3K/Akt inhibitor) showed that while both ROS blockade and PI3K/Akt pathway inhibition contributed to modulation of apoptosis,

ROS inhibition appeared to play a more dominant role. When NAC and LY294002 were co-treated, the resulting apoptosis levels were similar to those observed with NAC treatment alone, further supporting the hypothesis that ROS plays a more critical role than the PI3K/Akt pathway in regulating auranofin and SA-induced apoptosis. Therefore, we conclude that ROS is the primary mediator of apoptosis, with the PI3K/Akt pathway playing a secondary role. This suggests that targeting ROS could be a more effective strategy for enhancing the apoptotic response to auranofin and SA, whereas inhibition of the PI3K/Akt pathway may offer complementary benefits. While this study provides significant insights into the synergistic effects of auranofin and SA in HCC, several limitations should be considered. First, our findings are based on *in vitro* 2D and 3D spheroid models, which lack key physiological components such as immune interactions, vascularization, and tumor heterogeneity. Second, the use of a single HCC cell line limits the generalizability of our results, highlighting the need for validation in multiple HCC models with distinct molecular signatures. Third, although ROS and PI3K/Akt signaling were identified as key mediators of apoptosis, other mechanisms such as ferroptosis, necroptosis, and autophagy warrant further investigation. To build upon these findings, future studies could incorporate *in vivo* models, including patient-derived xenografts, to better assess the systemic efficacy and pharmacokinetics of auranofin and SA. Additionally, exploring alternative cell death pathways and potential resistance mechanisms may provide a more comprehensive understanding of their therapeutic potential. These efforts would help bridge the gap between preclinical research and clinical applications of auranofin and SA-based combination therapies for HCC.

In summary, our findings provided evidence that auranofin and SA act synergistically to inhibit Hep3B cell proliferation and induce apoptosis. The mechanism involved significant ROS generation and modulation of the PI3K/Akt signaling pathway (Figure 8). These insights offer valuable information for future therapeutic strategies aimed at utilizing oxidative stress and signaling pathway inhibitors to enhance the efficacy of cancer treatment. Further research into 3D organoids and the *in vivo* efficacy of these compounds is necessary to better assess their clinical potential.

Conflict of interest statement

The authors declare no potential conflicts of interest.

Funding

This work was supported by the National Research Foundation of Korea grant funded by the Korea government (RS-2023-00213236).

Data availability statement

The data supporting the findings of this study are available from the corresponding authors upon request.

Authors' contributions

HH and YHC conceived the project. HH, SYJ, and MYK contributed to the methodology. Both SYJ and MYK carried out the investigation. SHH and SOK were responsible for data curation. HH, SHH, SOK, and GYK performed the formal analysis. HH, GYK, and YHC wrote the original draft. HH, GYK, and YHC reviewed and edited the manuscript. YHC supervised the project. HH and YHC managed the project administration.

References

- [1] Llovet JM, Kelley RK, Villanueva A, Singal AG, Pikarsky E, Roayaie S, et al. Hepatocellular carcinoma. *Nat Rev Dis Primers* 2021; **7**(1): 6. doi: 10.1038/s41572-020-00240-3.
- [2] Foglia B, Turato C, Cannito S. Hepatocellular carcinoma: Latest research in pathogenesis, detection and treatment. *Int J Mol Sci* 2023; **24**(15). doi: 10.3390/ijms241512224.
- [3] Colquhoun SD, Wan YY. Hepatocellular carcinoma diagnosis and treatment: An overview. *Liver Res* 2020; **4**(4): 159-160. doi: 10.1016/j.livres.2020.11.006.
- [4] Gosalia AJ, Martin P, Jones PD. Advances and future directions in the treatment of hepatocellular carcinoma. *Gastroenterol Hepatol* 2017; **13**(7): 398-410.
- [5] Kojima-Yuasa A, Huang X, Matsui-Yuasa I. Synergistic anticancer activities of natural substances in human hepatocellular carcinoma. *Diseases* 2015; **3**(4): 260-281.
- [6] Wang Y, Li J, Xia L. Plant-derived natural products and combination therapy in liver cancer. *Front Oncol* 2023; **13**. doi: 10.3389/fonc.2023.1116532.
- [7] Rodriguez-Yoldi MJ. Anti-inflammatory and antioxidant properties of plant extracts. *Antioxidants (Basel)* 2021; **10**(6). doi: 10.3390/antiox10060921.
- [8] Wali AF, Majid S, Rasool S, Shehada SB, Abdulkareem SK, Firdous A, et al. Natural products against cancer: Review on phytochemicals from marine sources in preventing cancer. *Saudi Pharm J* 2019; **27**(6): 767-777.
- [9] Weng W, Goel A. Curcumin and colorectal cancer: An update and current perspective on this natural medicine. *Semin Cancer Biol* 2022; **80**: 73-86.
- [10] Ren B, Kwah MX, Liu C, Ma Z, Shanmugam MK, Ding L, et al. Resveratrol for cancer therapy: Challenges and future perspectives. *Cancer Lett* 2021; **515**: 63-72.
- [11] Aggarwal V, Tuli HS, Tania M, Srivastava S, Ritzer EE, Pandey A, et al. Molecular mechanisms of action of epigallocatechin gallate in cancer: Recent trends and advancement. *Semin Cancer Biol* 2022; **80**: 256-275.
- [12] Chen T, Xiao Z, Liu X, Wang T, Wang Y, Ye F, et al. Natural products for combating multidrug resistance in cancer. *Pharmacol Res* 2024; **202**. doi: 10.1016/j.phrs.2024.107099.
- [13] Abdalbari FH, Telleria CM. The gold complex auranofin: New perspectives for cancer therapy. *Discov Oncol* 2021; **12**(1): 42. doi: 10.1007/s12672-021-00439-0.
- [14] Chiappetta G, Gamberi T, Faienza F, Limaj X, Rizza S, Messori L, et al. Redox proteome analysis of auranofin exposed ovarian cancer cells (A2780). *Redox Biol* 2022; **52**. doi: 10.1016/j.redox.2022.102294.
- [15] Huang TL, Lin JC, Chyau CC, Lin KL, Chang CM. Purification of lignans from *Schisandra chinensis* fruit by using column fractionation and supercritical antisolvent precipitation. *J Chromatogr A* 2013; **1282**: 27-37.
- [16] Wan MLY, Turner PC, Co VA, Wang MF, Amiri KMA, El-Nezami H. Schisandrin A protects intestinal epithelial cells from deoxynivalenol-induced cytotoxicity, oxidative damage and inflammation. *Sci Rep* 2019; **9**(1). doi: 10.1038/s41598-019-55821-4.
- [17] Zhu L, Wang Y, Lv W, Wu X, Sheng H, He C, et al. Schizandrin A can inhibit non-small cell lung cancer cell proliferation by inducing cell cycle arrest, apoptosis and autophagy. *Int J Mol Med* 2021; **48**(6): 214. doi: 10.3892/ijmm.2021.5047.
- [18] Xiao Y, Zhou H, Cui Y, Zhu X, Li S, Yu C, et al. Schisandrin A enhances pathogens resistance by targeting a conserved p38 MAPK pathway. *Int Immunopharmacol* 2024; **128**. doi: 10.1016/j.intimp.2023.111472.
- [19] Guo X, Lei M, Ma G, Ouyang C, Yang X, Liu C, et al. Schisandrin A alleviates spatial learning and memory impairment in diabetic rats by inhibiting inflammatory response and through modulation of the PI3K/AKT pathway. *Mol Neurobiol* 2024; **61**(5): 2514-2529.
- [20] Jakubczyk K, Dec K, Kałduńska J, Kawczuga D, Kochman J, Janda K. Reactive oxygen species - sources, functions, oxidative damage. *Pol Merkur Lekarski* 2020; **48**(284): 124-127.
- [21] Sies H, Jones DP. Reactive oxygen species (ROS) as pleiotropic physiological signalling agents. *Nat Rev Mol Cell Biol* 2020; **21**(7): 363-383.
- [22] Brieger K, Schiavone S, Miller FJ Jr, Krause KH. Reactive oxygen species: From health to disease. *Swiss Med Wkly* 2012; **142**. doi: 10.4414/smw.2012.13659.
- [23] Nakamura H, Takada K. Reactive oxygen species in cancer: Current findings and future directions. *Cancer Sci* 2021; **112**(10): 3945-3952.
- [24] Wang H, Gao Z, Liu X, Agarwal P, Zhao S, Conroy DW, et al. Targeted production of reactive oxygen species in mitochondria to overcome cancer drug resistance. *Nat Commun* 2018; **9**(1): 562. doi: 10.1038/s41467-018-02915-8.
- [25] Perillo B, Di Donato M, Pezone A, Di Zazzo E, Giovannelli P, Galasso G, et al. ROS in cancer therapy: The bright side of the moon. *Exp Mol Med* 2020; **52**(2): 192-203.
- [26] Yang M, Liu J, Li J, Wen S, Hu Y, Lu W, et al. The rheumatoid arthritis

- drug auranofin exerts potent anti-lymphoma effect by stimulating TXNRD-mediated ROS generation and inhibition of energy metabolism. *Redox Biol* 2024; **75**. doi: 10.1016/j.redox.2024.103245.
- [27] Ni S, Qian Z, Yuan Y, Li D, Zhong Z, Ghorbani F, et al. Schisandrin A restrains osteoclastogenesis by inhibiting reactive oxygen species and activating Nrf2 signalling. *Cell Prolif* 2020; **53**(10). doi: 10.1111/cpr.12882.
- [28] Kang JB, Son HK, Park DJ, Jin YB, Koh PO. Chlorogenic acid regulates the expression of protein phosphatase 2A subunit B in the cerebral cortex of a rat stroke model and glutamate-exposed neurons. *Lab Anim Res* 2024; **40**(1): 8. doi: 10.1186/s42826-024-00196-5.
- [29] Jeon SJ, Jung GH, Choi EY, Han EJ, Lee JH, Han SH, et al. Kaempferol induces apoptosis through the MAPK pathway and regulates JNK-mediated autophagy in MC-3 cells. *Toxicol Res* 2024; **40**(1): 45-55.
- [30] Ni H, Hu X, Yang N, Liu X, Cai W, Zhong R, et al. Roundup® induces premature senescence of mouse granulosa cells via mitochondrial ROS-triggered NLRP3 inflammasome activation. *Toxicol Res* 2024; **40**(3): 377-387.
- [31] Jeon HJ, Seo JH, Jeong E, Son CY, Rawding PA, Hwang Y, et al. Carcinoembryonic antigen-positive circulating epithelial cells as a biomarker for the diagnosis and prognosis of colorectal cancer. *Biotechnol Bioprocess Eng* 2024; **29**(5): 877-889.
- [32] Kang GS, Kim YE, Oh HR, Jo HJ, Bok S, Jeon YK, et al. Hypoxia-inducible factor-1 α -deficient adipose-tissue macrophages produce the heat to mediate lipolysis of white adipose tissue through uncoupling protein-1. *Lab Anim Res* 2024; **40**(1): 37.
- [33] Xia Y, Sun M, Huang H, Jin WL. Drug repurposing for cancer therapy. *Signal Transduct Target Ther* 2024; **9**(1): 92. doi: 10.1038/s41392-024-01808-1.
- [34] Garg P, Malhotra J, Kulkarni P, Horne D, Salgia R, Singhal SS. Emerging therapeutic strategies to overcome drug resistance in cancer cells. *Cancers (Basel)* 2024; **16**(13). doi: 10.3390/cancers16132478.
- [35] Cui XY, Park SH, Park WH. Anti-cancer effects of auranofin in human lung cancer cells by increasing intracellular ROS levels and depleting GSH levels. *Molecules* 2022; **27**(16). doi: 10.3390/molecules27165207.
- [36] Ren X, Xue R, Luo Y, Wang S, Ge X, Yao X, et al. Programmable melanoma-targeted radio-immunotherapy via fusogenic liposomes functionalized with multivariate-gated aptamer assemblies. *Nat Commun* 2024; **15**(1): 5035. doi: 10.1038/s41467-024-49482-9.
- [37] Ye DJ, Kwon YJ, Baek HS, Cho E, Kwon TU, Chun YJ. Combination treatment with auranofin and nutlin-3a induces synergistic cytotoxicity in breast cancer cells. *J Toxicol Environ Health A* 2019; **82**(10): 626-637.
- [38] Zhang S, Zhao Y, Wang X, Qi C, Tian J, Zou Z. Synergistic lethality between auranofin-induced oxidative DNA damage and ATR inhibition in cancer cells. *Life Sci* 2023; **332**. doi: 10.1016/j.lfs.2023.122131.
- [39] Xu X, Rajamanicham V, Xu S, Liu Z, Yan T, Liang G, et al. Schisandrin A inhibits triple negative breast cancer cells by regulating Wnt/ER stress signaling pathway. *Biomed Pharmacother* 2019; **147**. doi: 10.1016/j.biopha.2022.112865.
- [40] Chen BC, Tu SL, Zheng BA, Dong QJ, Wan ZA, Dai QQ. Schizandrin A exhibits potent anticancer activity in colorectal cancer cells by inhibiting heat shock factor 1. *Biosci Rep* 2020; **40**(4). doi: 10.1042/BSR20200203.
- [41] Wang X, Wang F, Dong P, Zhou L. The therapeutic effect of ultrasound targeted destruction of schisandrin A contrast microbubbles on liver cancer and its mechanism. *Radiol Oncol* 2024; **58**(2): 221-233.
- [42] Freire Boullosa L, Van Loenhout J, Flieswasser T, Hermans C, Merlin C, Lau HW, et al. Auranofin synergizes with the PARP inhibitor olaparib to induce ROS-mediated cell death in mutant p53 cancers. *Antioxidants (Basel)* 2023; **12**(3). doi: 10.3390/antiox12030667.
- [43] Seo MJ, Kim IY, Lee DM, Park YJ, Cho MY, Jin HJ, et al. Dual inhibition of thioredoxin reductase and proteasome is required for auranofin-induced paraptosis in breast cancer cells. *Cell Death Dis* 2023; **14**(1): 42. doi: 10.1038/s41419-023-05586-6.
- [44] Fan J, Ren D, Wang J, Liu X, Zhang H, Wu M, et al. Bruceine D induces lung cancer cell apoptosis and autophagy via the ROS/MAPK signaling pathway *in vitro* and *in vivo*. *Cell Death Dis* 2020; **11**(2): 126. doi: 10.1038/s41419-020-2317-3.

Publisher's note

The Publisher of the *Journal* remains neutral with regard to jurisdictional claims in published maps and institutional affiliations.

Edited by Liang Q, Tan BJ

Supplementary Table. List of primary antibodies used for Western blot analysis.

Antibody	Source	Cat No.	Dilution
Akt	Santa Cruz Biotechnology	sc-81434	1:1 000
β -actin	Bioworld	BS6007M	1:20 000
Caspase-3	Santa Cruz Biotechnology	sc-7272	1:1 000
Caspase-8	Santa Cruz Biotechnology	sc-56070	1:1 000
Caspase-9	Santa Cruz Biotechnology	sc-56076	1:1 000
cIAP-1	Santa Cruz Biotechnology	sc-271419	1:1 000
p-Akt	Santa Cruz Biotechnology	sc-514032	1:1 000
p-PI3K	Cell Signaling Technology	4292S	1:1 000
PARP-1	Santa Cruz Biotechnology	sc-8007	1:1 000
PI3K	Cell Signaling Technology	4228S	1:1 000
XIAP	Proteintech	66800-1-Ig	1:1 000